Measurement of $\pi^- p \to \pi^0 \pi^0 n$ from threshold to $p_{\pi^-} = 750$ MeV/c

S. Prakhov,[1] B. M. K. Nefkens,[1] C. E. Allgower,[2,*] V. Bekrenev,[3] W. J. Briscoe,[4] M. Clajus,[1] J. R. Comfort,[5] K. Craig,[5] D. Grosnick,[6] D. Isenhower,[7] N. Knecht,[8] D. Koetke,[6] A. Koulbardis,[3] N. Kozlenko,[3] S. Kruglov,[3] G. Lolos,[8] I. Lopatin,[3] D. M. Manley,[9] R. Manweiler,[6] A. Marušić,[1,†] S. McDonald,[1,‡] J. Olmsted,[9,*] Z. Papandreou,[8] D. Peaslee,[10] N. Phaisangittisakul,[1] J. W. Price,[1] A. F. Ramirez,[5] M. Sadler,[7] A. Shafi,[4] H. Spinka,[2] T. D. S. Stanislaus,[6] A. Starostin,[1] H. M. Staudenmaier,[11] I. Supek,[12] and W. B. Tippens[1,§]

(Crystal Ball Collaboration)

[1]*University of California Los Angeles, Los Angeles, California 90095-1547, USA*
[2]*Argonne National Laboratory, Argonne, Illinois 60439-4815, USA*
[3]*Petersburg Nuclear Physics Institute, Gatchina 188350, Russia*
[4]*The George Washington University, Washington, D.C. 20052-0001, USA*
[5]*Arizona State University, Tempe, Arizona 85287-1504, USA*
[6]*Valparaiso University, Valparaiso, Indiana 46383-6493, USA*
[7]*Abilene Christian University, Abilene, Texas 79699-7963, USA*
[8]*University of Regina, Saskatchewan, Canada S4S OA2*
[9]*Kent State University, Kent, Ohio 44242-0001, USA*
[10]*University of Maryland, College Park, Maryland 20742-4111, USA*
[11]*Universität Karlsruhe, Karlsruhe 76128, Germany*
[12]*Rudjer Boskovic Institute, Zagreb 10002, Croatia*

(Received 28 October 2003; published 5 April 2004)

Reaction $\pi^- p \to \pi^0 \pi^0 n$ has been measured with high statistics in the beam momentum range 270–750 MeV/c. The data were obtained using the Crystal Ball multiphoton spectrometer, which has 93% of 4π solid angle coverage. The dynamics of the $\pi^- p \to \pi^0 \pi^0 n$ reaction and the dependence on the beam energy are displayed in total cross sections, Dalitz plots, invariant-mass spectra, and production angular distributions. Special attention is paid to the evaluation of the acceptance that is needed for the precision determination of the total cross section $\sigma_t(\pi^- p \to \pi^0 \pi^0 n)$. The energy dependence of $\sigma_t(\pi^- p \to \pi^0 \pi^0 n)$ shows a shoulder at the Roper resonance [i.e., the $N(1440)\frac{1}{2}^+$], and there is also a maximum near the $N(1520)\frac{3}{2}^-$. It illustrates the importance of these two resonances to the $\pi^0\pi^0$ production process. The Dalitz plots are highly nonuniform; they indicate that the $\pi^0\pi^0 n$ final state is dominantly produced via the $\pi^0\Delta^0(1232)$ intermediate state. The invariant-mass spectra differ much from the phase-space distributions. The production angular distributions are also different from the isotropic distribution, and their structure depends on the beam energy. For beam momenta above 550 MeV/c, the density distribution in the Dalitz plots strongly depends on the angle of the outgoing dipion system (or equivalently on the neutron angle). The role of the $f_0(600)$ meson (also known as the σ) in $\pi^0\pi^0 n$ production remains controversial.

DOI: 10.1103/PhysRevC.69.045202 PACS number(s): 13.75.Gx, 13.30.Eg, 14.20.Gk, 14.40.Cs

I. INTRODUCTION

When the πN center-of-mass (c.m.) energy is greater than 1.4 GeV, the major component of the πN total cross sections is due to the inelastic channels that are associated with nucleonic resonances. The principal inelastic channels are the pion production reactions $\pi N \to \pi\pi N$. Even not-so-heavy N^* and Δ^* resonances decay mainly by the $\pi\pi N$ channels rather than the phase-space-favored elastic way. For example, the branching ratio for the elastic channel of the $\Delta(1600)\frac{3}{2}^+$ is a mere 18%, while it is a hefty 82% for the decay into $\pi\pi N$ [1]. The study of the $\pi N \to \pi\pi N$ processes provides a valuable addition to the $\pi N \to \pi N$ elastic scattering partial-wave analyses that are used for determining the existence, the mass, the width, and decay channels of N^* and Δ^* resonances.

There exist some data on the $\pi^\pm p \to \pi\pi N$ charged channels; they have been analyzed using the isobar model [2–5]. In this model, the initial πN interaction produces simultaneously several N^* and Δ^* resonances that overlap in energy but have a different spin and/or parity. These N^*'s and Δ^*'s undergo quasi-two-body decays: (i) either into a pion plus a lighter isobar, which then decays further to the ground-state nucleon by emission of a second pion, (ii) or into a nucleon plus a dipion resonance, predominantly the ρ and, to a lesser extent, the f_0 meson. The amplitude for $\pi N \to \pi\pi N$ is a coherent sum of the amplitudes for the production of all the quasi-two-body channels.

*Present address: Indiana University Cyclotron Facility, 2401 Milo B. Sampson Ln., Bloomington, IN 47405, USA.
†Present address: Collider-Accelerator Dept., Brookhaven National Laboratory, Upton, NY 11973, USA.
‡Present address: TRIUMF, 4004 Wesbrook Mall, Vancouver, B.C., Canada V6T 2A3.
§Present address: Nuclear Physics Div., Dept. of Energy, 19901 Germantown Road, Germantown, MD 20874-1290, USA.

The interest in the study of $\pi\pi$ production at moderate energy has been stimulated recently by the speculation that the $\pi\pi$-production process could be dominated by the scalar-isoscalar $f_0(600)$ meson with quantum numbers $I(J^P)=0(0^+)$. The notation $f_0(600)$ is used by the Particle Data Group [1]. Historically, this state was known as the σ meson. There is speculation that the $f_0(600)$ has a smaller mass when it is produced inside nuclear matter [6,7]. This type of medium modification is a hoped-for signal for the onset of chiral symmetry restoration. A comprehensive study of the f_0 in $\pi\pi$ production at very low energy has been made in Ref. [8]; it is not conclusive on the role and the existence of this state.

The initial $\pi^- p$ system has two isospin components, $I_{1/2}$ and $I_{3/2}$, with $|\pi^- p\rangle = |\sqrt{\frac{1}{3}} I_{3/2} - \sqrt{\frac{2}{3}} I_{1/2}\rangle$. The final state may be characterized by $I(2\pi)$ and $I(N)$, with $I(2\pi)$ having the value 0, 1, and 2. For the $\pi^-\pi^+ n$ final state, $I(2\pi)$ is 0, 1, and 2, for $\pi^-\pi^0 p$ it is 1 and 2, and for $\pi^0\pi^0 n$ it is 0 and 2. According to several analyses of $\pi^-\pi^+ n$ and $\pi^-\pi^0 p$ production in the energy range under discussion [2–5], the dominant role is played by two resonances: $\rho(770) \to \pi\pi$ with $I(\rho)=1$ and $\Delta(1232) \to \pi N$ with $I(\Delta)=\frac{3}{2}$. The extraction of the resonance parameters and the contribution of the $f_0(600)$ from the $\pi^-\pi^+ n$ data is complicated. Since the $\pi^0\pi^0 n$ final state is free of any ρ contribution, it gives a unique opportunity for investigating the properties of the $f_0(600)$ and its role in $\pi\pi N$ production. So far the experimental data on these channels, especially $\pi^0\pi^0 n$, have been poor. This has hampered making a detailed partial-wave analysis.

In this article we present the results of extensive measurements of reaction

$$\pi^- p \to \pi^0\pi^0 n \tag{1}$$

from just above threshold at $p_{\pi^-}=265$ MeV/c to $p_{\pi^-}=750$ MeV/c. Important objectives of the experiment are to probe the dominant features of the reaction dynamics, to measure the total cross sections for reaction (1) with good precision, and to look whether there is the direct evidence of the Roper resonance in the cross-section energy dependence. We have measured reaction (1) at 19 incident beam momenta between 270 and 750 MeV/c, corresponding to c.m. energies 1212–1527 MeV. In this energy range, there are three well-established N^* states. The first one is the $N(1440)\frac{1}{2}^+$ (or the Roper resonance) with $\Gamma \approx 350$ MeV. The other two states are the $N(1520)\frac{3}{2}^-$ with $\Gamma \approx 120$ MeV and the $N(1535)\frac{1}{2}^-$ with $\Gamma \approx 150$ MeV. At our highest beam momenta, there is also expected to be a small contribution from a few Δ^* states, such as $\Delta(1600)\frac{3}{2}^+$, which we can ignore here. It is expected that the $\pi^0\pi^0 n$ final state is produced mainly by two sequential processes

$$\pi^- p \to N^* \to \pi^0\Delta^0(1232) \to \pi^0\pi^0 n \tag{2}$$

and

$$\pi^- p \to N^* \to f_0(600) n \to \pi^0\pi^0 n. \tag{3}$$

Note that process (2) involves two $\pi^0\Delta^0$ amplitudes due to the coupling of each of the two π^0's in the $\pi^0\pi^0 n$ final state to the neutron by the Δ isobar. The interference of these two $\pi^0\Delta^0$ amplitudes distorts the $\Delta^0 \to \pi^0 n$ decay angular distribution from its specific shape defined by the initial N^* state. From threshold to $p_{\pi^-}=660$ MeV/c, the dominant N^* isobar in processes (2) and (3) is the $N(1440)\frac{1}{2}^+$; at higher beam momenta, they are the $N(1520)\frac{3}{2}^-$ and the $N(1535)\frac{1}{2}^-$. The decay to $\pi^0\Delta^0$ goes by P wave for the $N(1440)\frac{1}{2}^+$, by S and D waves for the $N(1520)\frac{3}{2}^-$, and by D wave for the $N(1535)\frac{1}{2}^-$. The decay to $f_0(600)n$ goes by S wave for the $N(1440)\frac{1}{2}^+$, and by P wave for both the $N(1520)\frac{3}{2}^-$ and the $N(1535)\frac{1}{2}^-$.

An earlier version of the analysis of our experiment has been presented in Ref. [9], where a multipole decomposition into spherical harmonics of the dipion decay angular distributions was given. It shows that the $f_0(600)$ is not produced by a one-pion-exchange mechanism, and that $\pi^0\pi^0 n$ production is dominated by sequential π^0 decays through the $\Delta(1232)$ resonance.

II. EXPERIMENTAL SETUP

The measurement of $\pi^- p \to \pi^0\pi^0 n$ was performed at Brookhaven National Laboratory with the Crystal Ball (CB) multiphoton spectrometer, which was installed in the C6 beam line of the Alternating Gradient Synchrotron. The Crystal Ball consists of 672 optically isolated NaI(Tl) crystals, shaped like truncated triangular pyramids and arranged in two hemispheres covering 93% of 4π steradians. The pulse height in every crystal was measured using an individual analog-to-digital converter (ADC). For registering the timing information, one TDC was used for every minor triangle, which is a group of nine neighboring crystals. The typical energy resolution for electromagnetic showers in the CB was $\Delta E/E = 0.020/(E[\mathrm{GeV}])^{0.36}$. Shower directions were measured with a resolution in θ, which is the polar angle with respect to the beam axis, to be $\sigma_\theta = 2° - 3°$ for photon energies in the range 50–500 MeV, assuming that the photons are produced in the center of the CB. The resolution in azimuthal angle ϕ is $\sigma_\theta/\sin\theta$. The angular resolutions are mainly defined by the granularity of the CB. When the event does not occur in the center of the CB, the angular resolution of a particular photon also depends on the distance for this photon from the event origin to the inner surface of the CB, on the angle at which the photon hits the crystal surface, and on the effective depth of the electromagnetic shower in the NaI(Tl) material. This effective depth was used as the pivot in the calculation of the photon angles from the vertex coordinates.

The experiment was performed with a momentum-analyzed beam of negative pions. The mean values p_{π^-} of the incident-momentum spectra and the momentum spread σ_p at the CB target are listed for all experimental data in Tables I and II (see the section with results for cross sections). The mean momentum of the beam spectrum at the target center

TABLE I. Summary of the main results for the total cross section of reaction $\pi^- p \to \pi^0\pi^0 n$. Content of columns: (1) beam momentum and its spread, (2) number of $\pi^- p \to \pi^0\pi^0 n$ candidates, (3) number of $\pi^0\pi^0 n$ events remaining after background subtraction, (4) total cross section $\sigma_t(\pi^- p \to \pi^0\pi^0 n)$, where the uncertainties are statistical only.

$p_{\pi^-} \pm \sigma_p$ (MeV/c)	N_{Expt}	$N_{\pi^0\pi^0 n}$	$\sigma_t(\pi^- p \to \pi^0\pi^0 n)$ (mb)
271±3	1	1	0.00025±0.00025
298±3	56	54	0.0093±0.0013
322±3	153	149.5	0.0270±0.0024
355±4	482	457	0.0830±0.0042
373±4	5248	4979	0.131±0.002
404±4	7290	7035	0.244±0.003
472±5	10672	10296	0.725±0.008
501±5	2479	1855	0.969±0.030
550±5	41282	40158	1.301±0.009
612±6	5428	3960	1.514±0.035
656±6	63801	61585	1.629±0.010
668±6	34285	32928	1.689±0.013
678±6	33496	32347	1.761±0.013
691±6	30239	29100	1.880±0.015
704±7	57078	55138	2.073±0.013
719±7	28288	27408	2.132±0.018
727±7	34338	33218	2.156±0.017
733±6	30216	29210	2.195±0.018
748±7	30379	29352	2.144±0.019

was known with a precision of 2–3 MeV/c. The first part of the experiment was completed in 1998 using a 10-cm-long liquid hydrogen (LH_2) target located in the center of the CB. High statistics data were taken at each beam momentum. An inconsistency in the determination of the beam contamination by electrons became apparent during the analysis; therefore, to obtain absolute cross sections, the data had to be separately normalized. For this purpose, a follow-up of the experiment was done in 2002 after improving the pion beam and refining its triggering. Also, a set of solid targets, 1-, 2- and 3-cm-thick, was used instead of the 10-cm-long LH_2 target. The diameter of all solid targets, as well as the LH_2 target, was about 10 cm. In the case of the solid targets, the pion interactions in hydrogen were measured using CH_2 targets. The background due to pion interactions in carbon was measured using pure carbon targets. The thickness of the carbon targets was chosen in such a way that the energy loss of the beam pion in them was the same as in the corresponding CH_2 target. The beam trigger was a coincidence between three scintillation counters located in the beam line upstream of the CB. The CB event trigger was the beam trigger in coincidence with a Crystal Ball signal, which included the requirement that the total energy deposited in the crystals exceeded a certain threshold. The neutral-event trigger required the anticoincidence of the CB event trigger with signals from a barrel of scintillation counters surrounding the target. More details about the CB detector and the data analyses can be found in Refs. [10,11].

III. DATA HANDLING

To select candidates for reaction

$$\pi^- p \to \pi^0\pi^0 n \to 4\gamma n, \tag{4}$$

we used the neutral four-cluster and five-cluster events, where we have assumed that each photon produced a shower in the CB. In the case of the four-cluster events, the missing particle was assumed to be the neutron. For the five-cluster events, one of the clusters was considered to be from the neutron interaction in the CB. The "cluster" algorithm was optimized to determine a group of neighboring crystals in which energy was deposited from a single-photon electromagnetic shower. The software threshold of the cluster energy was chosen to be 14 MeV; this value optimizes the number of the reconstructed events of reaction (4). All events were subjected to a kinematic fit to test the hypothesis of being reaction (4). The measured parameters in the kinematic fit included five for the beam particle (momentum, angles θ_x and θ_y, and position coordinates x and y on the target) and three for each photon cluster (energy, angles θ and ϕ). When the missing particle was the neutron, its energy and two angles were free parameters in the fit. For the neutron detected by the CB, the neutron angles were used as the measured parameters. In the cases of the data taken with the 10-cm-long LH_2 target, the z coordinate of the vertex was a free parameter of the kinematic fit. For the solid target, the z coordinate was assumed to be the measured parameter of the fit. The initial value of this parameter was the z coordinate of the target center, and the parameter variance was one third of the target thickness. The cluster angles θ and ϕ that are used in the minimization procedure were calculated with respect to the center of the CB. To determine the kinematic constraints, the cluster angles were recalculated to find the real angles of the photons and the neutron by using a transformation to the vertex coordinates. The pivot for the rotation of the cluster angles was chosen to be the effective depth of the electromagnetic shower in the NaI material. In the present analysis, the effective depth of the electromagnetic shower was defined as the depth where the photon has likely deposited half its initial energy. For the neutron cluster, the effective depth was taken to be half the length of the crystals.

In addition to the four main constraints of the kinematic fit, which are based on energy and three-momentum conservation, there are two extra constraints that require the invariant mass of each photon-photon pair to be the known π^0-meson mass. The total number of constraints for the hypothesis of reaction (4) is six. The effective number of constraints is smaller by the number of free parameters of the fit. In case of the solid targets, it is a 3-C and 5-C fit for four-cluster and five-cluster events, respectively. For the LH_2 data, where the z coordinate is a free parameter of the fit, it is correspondingly a 2-C and 4-C fit. The kinematic fit was performed for every possible pairing combination of four photons to form two π^0's. For four-cluster events, there are three such permutations of the four photons. In case of five-cluster events, this number is five times larger, since the neu-

TABLE II. Supplementary results from the CH_2 data, used for studying systematic uncertainties. Content of columns: (1) beam momentum and its spread, (2) thickness of the CH_2 target, (3) z coordinate of the CH_2 target with respect to the CB center, (4) number of $\pi^- p \to \pi^0\pi^0 n$ candidates, (5) number of $\pi^0\pi^0 n$ events remaining after background subtraction, (6) total cross section $\sigma_t(\pi^- p \to \pi^0\pi^0 n)$, where the uncertainties are statistical only. The four data sets with the momentum marked by the symbol * were taken with different beam collimation that resulted in a larger fraction of empty-target background.

$p_{\pi^-} \pm \sigma_p$ (MeV/c)	l_{CH_2} (cm)	z_{CH_2} (cm)	$N_{\text{Expt.}}$	$N_{\pi^0\pi^0 n}$	$\sigma_t(\pi^- p \to \pi^0\pi^0 n)$ (mb)
471±5	2	0	924	667	0.690±0.037
550±5	2	0	5986	4568	1.324±0.027
656±6	3	0	8767	6308	1.680±0.032
657±6	2	0	4688	3347	1.708±0.045
658±6	1	0	1825	1307	1.604±0.062
681±7	2	0	6567	4752	1.793±0.038
694±7	2	0	7437	5272	1.816±0.039
*694±7	2	−17.5	2836	1994	2.006±0.064
*707±7	2	−17.5	2927	1958	1.933±0.064
709±7	2	0	4952	3564	2.036±0.051
*720±7	2	−17.5	2653	1912	2.186±0.070
721±7	2	−17.5	3172	2218	2.088±0.067
724±7	2	0	9588	6845	1.953±0.038
738±7	3	0	7255	5151	2.195±0.047
738±7	3	−16	6293	4434	2.277±0.048
741±7	1	0	4899	3501	2.179±0.056
753±7	2	0	5825	4148	2.109±0.051
753±7	2	−17.5	4068	2786	2.153±0.061
*753±7	2	−17.5	3171	2188	2.108±0.063

tron cluster is also involved in the permutations. Events for which at least one pairing combination satisfied the hypothesis of reaction (4) at the 2% confidence level (C.L.) (i.e., with a probability greater than 2%) were accepted as $\pi^0\pi^0 n$ event candidates. A tighter cut on the C.L. is unnecessary, as there is almost no background. The pairing combination with the largest C.L. was used to reconstruct the kinematics of the reaction.

Since the decay time of NaI(T1) is about 250 ns, there is a possibility of finding one or more clusters that do not belong to the event which caused the CB trigger. The fraction of these pileup clusters increases with the increase of the beam intensity. The crystals near the beam line in the entrance and exit tunnels are more contaminated with pileup clusters, which are mostly muons from the decay of pions in the beam, or pions that have scattered in the material of the detector. The pileup clusters, unless they are eliminated, change the cluster multiplicity of true events. As a consequence, such events are lost in the analysis. The elimination of the pileup clusters is based on the TDC information of the crystals forming the clusters. All clusters that occur outside the proper TDC gate were eliminated from further consideration. This procedure is very efficient. Some small losses occur only if the true cluster overlaps with the pileup one. From a comparison of the data samples taken at different beam intensity, it was deduced that these losses vary from zero to a few percent. In our final analysis we tried to use only data sets that had been taken at low enough beam intensity, i.e., where such losses were less than 1%.

The events selected as $\pi^- p \to \pi^0\pi^0 n$ have almost no background from other final states. There are only two other channels in our energy range that have a large cross section: $\pi^- p \to \pi^0 n$ and $\pi^- p \to \eta n$. Using a simulation of $\pi^0 n$, $\eta n \to \gamma\gamma n$, and $\eta n \to 3\pi^0 n$ events, we estimate that the contamination due to their misidentification as $\pi^0\pi^0 n$ events is much less than 1%. The production of the $3\pi^0 n$ final state that is not due to an η decay has a very small cross section at these energies [12], so that we neglected this contribution.

Another source of background comes from processes that are not pion interactions in the hydrogen of the target. The main contributions to this background are from beam pions that can decay or scatter before reaching the target, or can interact in the material surrounding the target or in the carbon nuclei of the CH_2 target. The background events that were not associated with an interaction in the carbon nuclei of the CH_2 target were investigated using data samples of an empty target. The absolute fraction of this background was determined using the ratio of the total number of beam pions N_{π^-} incident on the target for the data taken with full and empty target. The fraction of the so-called "empty-target" background varies for different data sets mostly between 2% and 4%. The "carbon" background was determined by analysis of data samples obtained with the carbon target. The procedure was identical to the one that was used for the analysis of the CH_2 target. To determine the absolute contribution of the carbon data, which have to be subtracted from the CH_2,

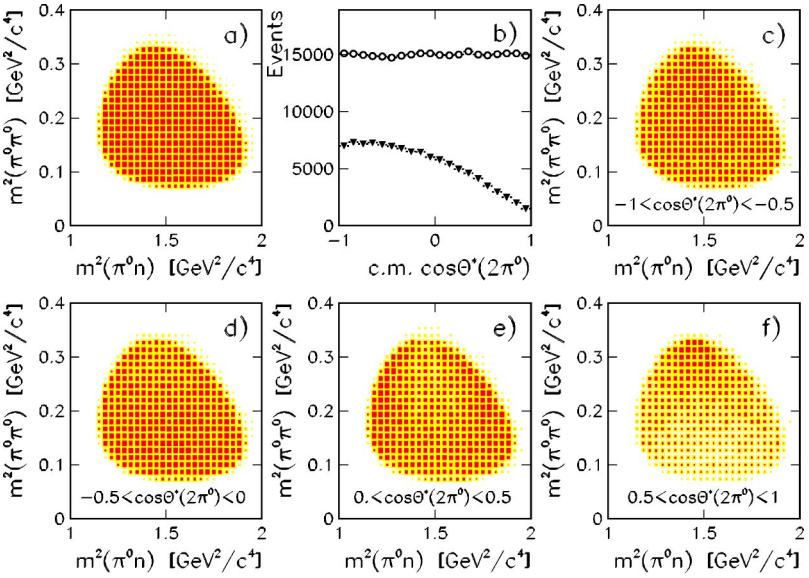

FIG. 1. (Color online) MC results for our investigation of the features of the CB acceptance for reaction $\pi^- p \to \pi^0 \pi^0 n$: (a) Dalitz plot of 3×10^5 phase-space events simulated for $p_{\pi^-} = 733$ MeV/c and the LH_2 target; (b) the phase-space input (circles) and CB-accepted (triangles) events as a function of cos θ^*, Dalitz plot of the accepted events divided in four subsets: (c) $-1 <$ cos $\theta^* < -0.5$, (d) $-0.5 <$ cos $\theta^* < 0$, (e) $0 <$ cos $\theta^* < 0.5$, and $-0.5 <$ cos $\theta^* < 1$.

we used the ratio of the beam N_{π^-} for the CH_2 and the carbon target, adjusted by the ratio of the carbon nuclei in both targets. The typical fraction of the carbon background for the $\pi^0 \pi^0 n$ events from the CH_2 target was about 25%–28%. The number of the experimental events selected for reaction (1) at each beam momentum is listed in Tables I and II as N_{Expt}. The number of the $\pi^0 \pi^0 n$ events remaining after the background subtraction is listed in these tables as $N_{\pi^0 \pi^0 n}$. All numbers correspond to the sum of four-cluster and five-cluster events. The fraction of five-cluster events strongly depends on the neutron momentum in the lab system. At the lowest beam momenta, it is less than 1%; at $p_{\pi^-} = 750$ MeV/c, it is about 17%.

IV. ACCEPTANCE EVALUATION

To calculate the total cross section for reaction (1), one has to know the number of the $\pi^0 \pi^0 n$ events that were initially produced during the beam exposure. Since our reaction has a three-body final state, its dynamics can be described by five kinematic variables. The appropriate set of such variables includes beam momentum, two invariant masses of the particles in the final state, and two production angles, θ^* and ϕ^*, for one of the particles in the c.m. system. The experimental acceptance for the reaction may also depend on these kinematic variables; and for the correct calculation of the number of initially produced $\pi^0 \pi^0 n$ events, these dependences must be taken into account. To study the acceptance dependence on the invariant masses, we used the Dalitz plot of $m^2(\pi^0 \pi^0)$ versus $m^2(\pi^0 n)$, where $m(\pi^0 \pi^0)$ and $m(\pi^0 n)$ are the invariant mass of the $\pi^0 \pi^0$ and $\pi^0 n$ system, respectively. Since there are two possible $\pi^0 n$ systems, every event has two entries in the Dalitz plot. For studying the acceptance dependence on the production angles, the convenient choice is to take the neutron angles. Choosing the individual π^0 angles would lead to the ambiguity of which of the two π^0's in the final state to use. In our study we used the production angles for the $2\pi^0$ system, for which the direction in the overall c.m. system is just opposite to the neutron direction. The strongest dependence of the CB acceptance was expected to be on θ^*, which was defined as the angle between the $2\pi^0$ direction and the beam direction in the overall c.m. system. Due to the 4π CB geometry, the acceptance dependence on ϕ^* must be very small.

To determine the acceptance, we performed a Monte Carlo (MC) simulation of $\pi^- p \to \pi^0 \pi^0 n$ events in accordance with phase-space distributions. The simulation was made for each experimental momentum using the experimental beam-trigger events as input for the pion-beam distributions. The MC events were then propagated through a full GEANT (version 3.21) simulation of the CB detector, folded with the CB resolutions and trigger conditions, and analyzed the same way as the experimental data. The small difference between the data and MC for the neutron response in the CB was not important, as we analyzed the four-cluster and five-cluster events together. According to the analysis of the simulated samples, the average detection efficiency for the phase-space $\pi^- p \to \pi^0 \pi^0 n$ events is between 30% and 40%, depending on the beam momentum and other experimental conditions. This is only half of the geometrical acceptance of the CB for four photons, which is $(0.93)^4 = 0.75$. The first reason for a decrease of the acceptance is the forward boost of the final-state photons in the lab system in conjunction with the hole in the CB for the beam exit; the higher the beam momentum the smaller the acceptance. The second reason is photon interactions in the beam pipe and in the barrel of scintillation counters surrounding the target. Usually such events do not satisfy the trigger for a neutral CB event. According to the simulation, the average probability for one photon not to pass the neutral-trigger requirement is about 6%, or 24% for four photons. Finally, there is some inefficiency in cluster reconstruction, when either the cluster energy is below threshold or clusters overlap.

The dependence of the CB acceptance on the invariant-mass squared $m^2(\pi^0 \pi^0)$ and $m^2(\pi^0 n)$, and on the dipion production angle θ^* is illustrated in Fig. 1 by the corresponding Dalitz plots and the cos θ^* distributions. The simulated Dalitz plot for 3×10^5 events of reaction (1) at p_{π^-}

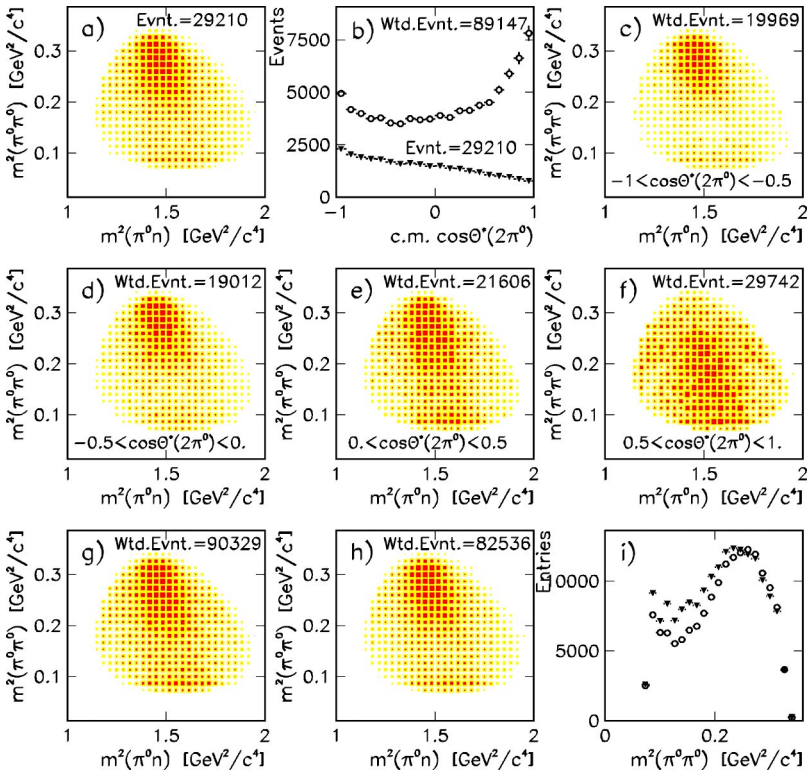

FIG. 2. (Color online) The effect of the acceptance correction on the experimental $\pi^0\pi^0 n$ distributions for the LH_2 data at $p_{\pi^-}=733$ MeV/c: (a) the Dalitz plot obtained after the empty-target background subtraction, (b) the cos θ^* spectrum before (triangles) and after the acceptance correction (circles), the acceptance-corrected Dalitz plots for four subsets: (c) $-1<\cos\theta^*<-0.5$, (d) $-0.5<\cos\theta^*<0$,(e) $0<\cos\theta^*<0.5$, and (f) $0.5<\cos\theta^*<1$, (g) the sum of the four plots shown in (c), (d), (e), and (f), (h) the Dalitz plot obtained as a result of the correction by the overall acceptance. (i) Triangles are the $m^2(\pi^0\pi^0)$ projection of the Dalitz plot of (g), and circles are the same for the Dalitz plot of (h).

$=733$ MeV/c with the LH_2 target is shown in Fig. 1(a). Since the simulation was performed in accordance with phase space, the initial Dalitz plot and cos θ^* distribution must have uniform density.

The decrease of the event population on the Dalitz plot contour is just a reflection of the beam momentum spread. The simulated cos θ^* distribution, obtained for the same MC sample, is shown in Fig. 1(b) by circles. The corresponding distribution, which was obtained from the analysis of the MC sample, is shown in the same figure by triangles. The ratio of this distribution to the simulated one is the cos θ^* acceptance. It is seen that the CB acceptance for $\pi^0\pi^0 n$ events drops by a factor of 4 from backward to forward $2\pi^0$ production. It is a consequence of the forward boost of the final-state photons in the lab system. When both π^0's are produced in the forward direction, the probability for at least one of the four photons to escape through the downstream beam hole is the largest. The Dalitz plot acceptance was investigated for different regions of cos θ^*. In Figs. 1(c)–1(f) we show four Dalitz plots for the reconstructed events divided in four subsets depending on the cos θ^* value. It is seen that for $\cos\theta^*<0.5$, the Dalitz plot acceptance is almost uniform; for forward angles (i.e., when $\cos\theta^*>0.5$), the acceptance decreases for small masses of the $2\pi^0$ system. This effect is not unexpected, since the $2\pi^0$ system with a small invariant mass has a small opening angle between the two π^0's. In that case, both the π^0's fly almost along the direction of the $2\pi^0$ system, i.e., towards the downstream beam hole where the probability for the decay photons to escape is the largest. For backward $2\pi^0$ angles, this effect is almost canceled by the forward boost of the π^0's in the lab system.

We have tested three approaches for adjusting the experimental distributions by the acceptance; they are illustrated in Fig. 2. In Fig. 2(a) we show the experimental Dalitz plot for the 29210 $\pi^0\pi^0 n$ good events that were left after subtraction of the empty-target background. The data were taken with the LH_2 target at $p_{\pi^-}=733$ MeV/c; this energy is near the maximum of the $N(1520)\frac{3}{2}^-$ resonance. In Fig. 2(b) for the same experimental events, we give the cos θ^* spectrum (shown by triangles).

The acceptance-corrected cos θ^* spectrum, which is shown in the same figure by circles, contains 89147 weighted events (i.e., the number of events in the spectrum after the acceptance correction). One can see that the dipion production angular distribution is far from isotropic, and the forward production is the largest. The result of dividing the data in four subsets depending on the cos θ^* value is illustrated in Figs. 2(c)–2(g); we show here four experimental Dalitz plots corrected by their acceptances, and also the Dalitz plot that is obtained as the sum of these four plots. The latter Dalitz plot contains 90329 weighted events; this number compared to the first approach is larger by 1.3%. The difference of 1.3% between the two methods may be considered as reasonable agreement of these approaches. The result of correcting the experimental Dalitz plot from Fig. 2(a) by its overall acceptance, which is shown in Fig. 2(h), yields only 82536 weighted events; it is similar to the number that would have been obtained if we use just the mean detection efficiency for the acceptance correction. The density distribution of the experimental Dalitz plot before and after the overall acceptance correction is very similar as well. It is seen that the third method underestimates the number of initially produced events by about 8%. It happens because the large $2\pi^0$ production in the forward angles occurs in the region of the smallest acceptance. The third method also underestimates the number of events at low $m(\pi^0\pi^0)$ invariant

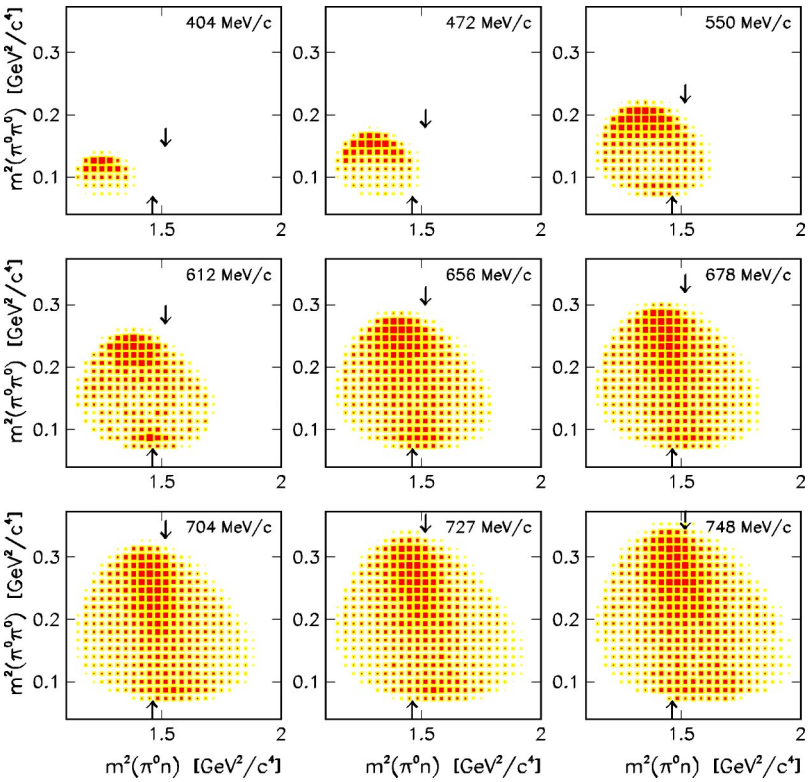

FIG. 3. (Color online) The acceptance-corrected Dalitz plots of $m^2(\pi^0\pi^0)$ vs $m^2(\pi^0 n)$ for the experimental events of reaction $\pi^- p \to \pi^0\pi^0 n$ at nine beam momenta. The arrow pointing up at $m^2(\pi^0 n)=(1.21)^2$ GeV$^2/c^4$ in each plot shows the real part of the pole for the Δ resonance. The arrow pointing down at $m^2(\pi^0 n)=(1.232)^2$ GeV$^2/c^4$ marks the conventional value for the Breit-Wigner mass of the Δ.

mass. In Fig. 2(i) we compare the $m^2(\pi^0\pi^0)$ projection of the acceptance-corrected Dalitz plots obtained by the second and third methods. It is seen that at low $m(\pi^0\pi^0)$ masses, the yield of events from the third method (shown by circles) is significantly smaller than the one from the second method (shown by triangles).

For every beam momentum where the experimental statistics allowed it, we tested all three methods for the acceptance correction. It was found that the first and second methods agreed better for all data with beam momentum above $p_{\pi^-}=550$ MeV/c. For beam momenta at and below $p_{\pi^-}=550$ MeV/c, all three methods gave nearly the same number of initially produced $\pi^0\pi^0 n$ events. Finally, to obtain our results for the $\pi^0\pi^0 n$ cross sections, we used the first method of the acceptance correction (i.e., the method of the cos θ^* distribution). For the two lowest beam momenta ($p_{\pi^-}=271$ MeV/c and 298 MeV/c), where the experimental statistics is very small, the average acceptance correction was applied.

V. FEATURES OF THE DATA

In Fig. 3 we show the $\pi^0\pi^0 n$ Dalitz plots for nine beam momenta that cover our full energy range. All Dalitz plots are background subtracted and acceptance corrected. The acceptance correction was made according to our second method, i.e., by dividing the data into four equal intervals in cos θ^*, and correcting each of the four Dalitz plots by its acceptance. All Dalitz plots but one in Fig. 3 are for the LH_2 data. The LH_2 data have more statistics and less background than the CH_2 data, which are shown here only for one momentum, $p_{\pi^-}=612$ MeV/c, that was not taken with the LH_2 target.

Figures 4 and 5 show the projections of these plots on the $m^2(\pi^0 n)$ and $m^2(\pi^0\pi^0)$ axes, respectively. The $\pi^0\pi^0 n$ phase-space distributions are shown in the same figures by the dashed curves. These distributions are normalized to the number of experimental events.

To interpret the experimental Dalitz plots and their projections, let us note certain revealing features of these distributions. The manifestation of the $\Delta(1232)$ produced by process (2) is clearly seen in Figs. 3 and 4.

The maximum of the Δ peak occurs close to the real part of the pole position of the Δ resonance, which is 1210 MeV [1]. This is expected, as the conventional Breit-Wigner mass of the Δ, which is 1232 MeV, is determined from the analysis of πN elastic scattering, where the fit to the P33 partial wave has a large background from the nucleon pole term. In our case we have a three-body final state where the Δ isobar is produced as an intermediate state. In Figs. 3 and 4 the pole position is shown by the arrow pointing up, and the conventional Breit-Wigner mass is shown by the arrow pointing down. Some changes that are seen in the Δ's shape for different momenta can be explained by the fact that for every $\pi^0 n$ system produced due to Δ decay, there is the second $\pi^0 n$ system, the invariant mass of which smears the Δ's signal in the plots. Since the $\pi^0\pi^0 n$ system has two identical particles, the Dalitz plot has a line of symmetry. This line connects the points on the Dalitz plot contour that have the largest and the smallest invariant-mass squared $m^2(\pi^0\pi^0)$. Every event has two entries in the Dalitz plot, which have the same $m^2(\pi^0\pi^0)$ but two different $m^2(\pi^0 n)$. It is a property of the $\pi^0\pi^0 n$ Dalitz plot that these two entries lie opposite to the line of symmetry and at the same distance to it. In Fig. 6 we illustrate this property of the $\pi^0\pi^0 n$ Dalitz plot using simulated events of the hypothetical process $\pi^- p \to \pi_1^0 \Delta^0 \to \pi_1^0 \pi_2^0 n$,

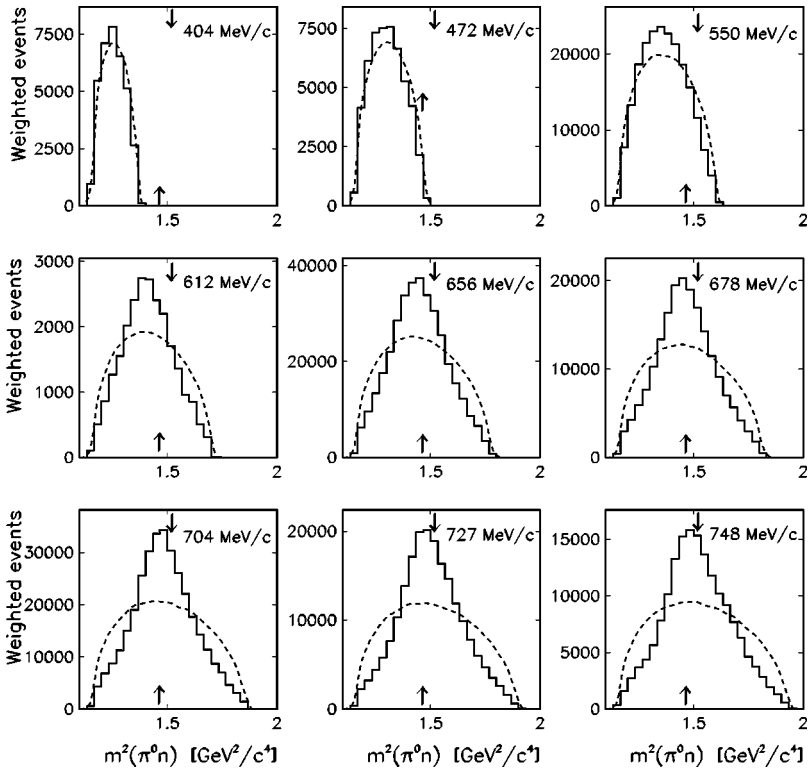

FIG. 4. The $m^2(\pi^0 n)$ projections of the Dalitz plots shown in Fig. 3. The arrow pointing up at $m^2(\pi^0 n)=(1.21)^2$ GeV$^2/c^4$ shows the real part of the pole for the Δ resonance. The arrow pointing down at $m^2(\pi^0 n)=(1.232)^2$ GeV$^2/c^4$ marks the conventional value for the Breit-Wigner mass of the Δ. The dashed curves show the $\pi^0\pi^0 n$ phase-space distributions normalized to the number of the experimental events.

where each π^0 has an extra subscript. The beam conditions for the simulated events are identical to the data at $p_{\pi^-}=748$ MeV/c. The Δ mass of 1210 MeV and the width of 100 MeV were taken according to the pole position of the Δ resonance [1]. Knowing now which π^0 is from the Δ decay, we can distinguish the distributions for the two $\pi^0 n$ systems. In Fig. 6(a), the Dalitz plot is shown for $m(\pi_2^0 n)$ only; this choice selects the Δ decay. In Fig. 6(b) one can see that the choice of $m(\pi_1^0 n)$ results in the reflection of the Δ's band with respect to the line of symmetry. The Dalitz plot in Fig. 6(c) is the sum of the two first figures. In Figs. 6(d)–6(f) we show the $m^2(\pi^0 n)$ projection for each of the three Dalitz plots.

A visual examination of the nine Dalitz plots and their

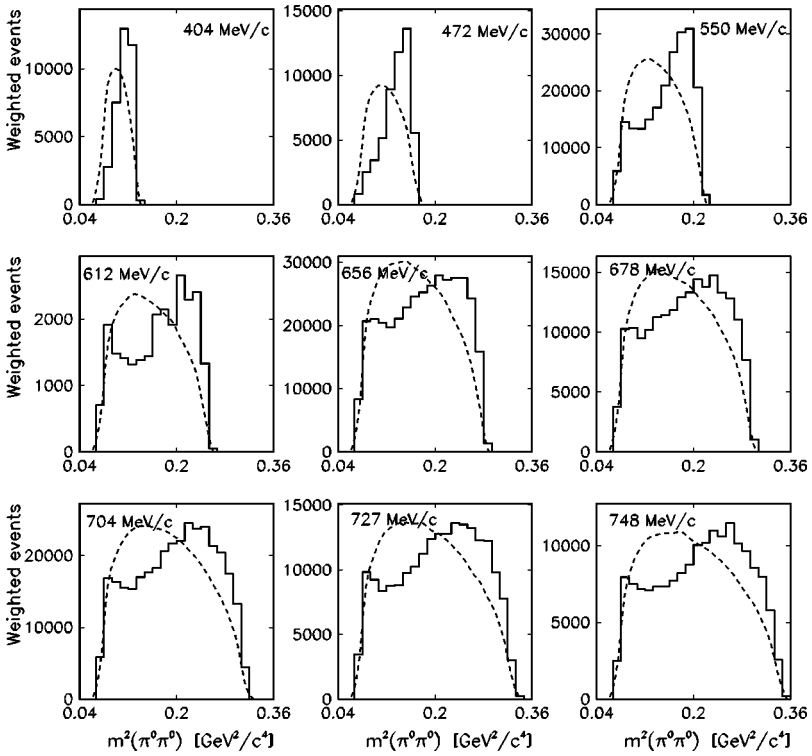

FIG. 5. The $m^2(\pi^0\pi^0)$ projections of the Dalitz plots shown in Fig. 3. The dashed curves show the $\pi^0\pi^0 n$ phase-space distributions normalized to the number of the experimental events.

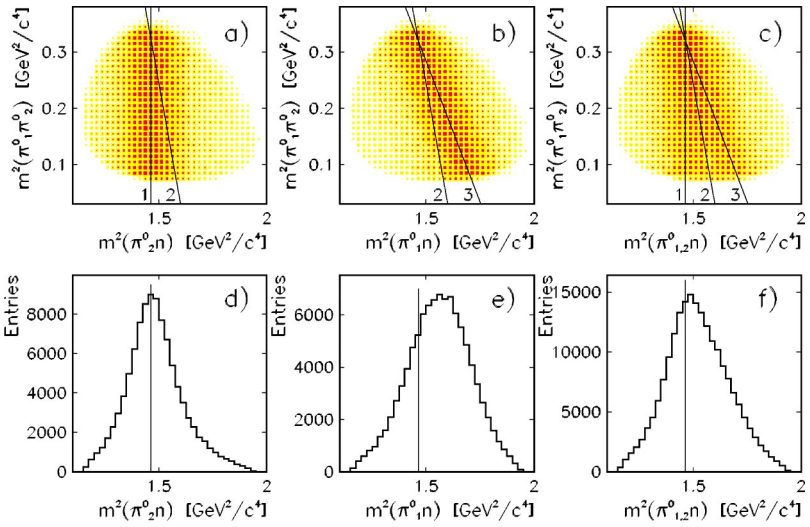

FIG. 6. (Color online) Dalitz plots and their $m^2(\pi^0 n)$ projections for Monte Carlo events of the sequential process $\pi^- p \to \pi_1^0 \Delta^0 \to \pi_1^0 \pi_2^0 n$ at $p_{\pi^-}=748$ MeV/c: (a) $m^2(\pi_1^0\pi_2^0)$ vs $m^2(\pi_2^0 n)$, (b) $m^2(\pi_1^0\pi_2^0)$ vs $m^2(\pi_1^0 n)$, (c) $m^2(\pi_1^0\pi_2^0)$ vs $m^2(\pi_{1,2}^0 n)$, (d) $m^2(\pi_2^0 n)$, (e) $m^2(\pi_1^0 n)$, and (f) $m^2(\pi_{1,2}^0 n)$. The vertical line at $(1.21)^2$ GeV^2/c^4 corresponds to the real part of the pole for the Δ resonance; this mass was used in the simulation. Line number 2 is the line of symmetry of the Dalitz plot that connects the points on the Dalitz plot contour which have the largest and the smallest mass $m^2(\pi^0\pi^0)$. Line number 3 is a reflection of the vertical line number 1 with respect to the line of symmetry (i.e., line number 2).

projections does not allow a quantitative conclusion about the size of the f_0-meson contribution, except that it is not the major one. If the f_0 meson, produced by process (3), had a mass of 600 MeV or below, and a width of 200–300 MeV, it would be seen as a horizontal band in our Dalitz plots. In Ref. [1] the $f_0(600)$ meson is listed as having a width of 600–1000 MeV. Such a broad state would look like an almost uniform distribution in our plots; however, a uniform-density component does not appear to be a major part of our $\pi^0\pi^0 n$ data. A horizontal band with a narrower width is seen at the top of the Dalitz plots of the low-momentum data. It seems to be produced by Δ and its reflection with respect to the symmetry line rather than by the f_0 meson. If it were a signal from f_0, this band would be centered around the same $m(\pi^0\pi^0)=m_\sigma$, have the same width of Γ_{f_0}, and be seen for our higher beam momenta as well.

The general feature of the $\pi^0\pi^0 n$ data for all beam momenta is a strong asymmetry in population of the events along the invariant mass of the $\pi^0\pi^0$ system. The number of $\pi^0\pi^0 n$ events with large $m(\pi^0\pi^0)$ masses is considerably larger than with small ones. For a better illustration of the magnitude of this asymmetry, we show in Fig. 7 the ratio of the experimental $m^2(\pi^0\pi^0)$ spectrum and its phase-space distribution for the nine beam momenta shown in Fig. 5.

A likely explanation for such an asymmetry is the interference of the transition amplitudes.

Another interesting feature of the $\pi^0\pi^0 n$ events became apparent when the data were divided into four Dalitz plots according to the $\cos\theta^*$ value. For the data at $p_{\pi^-}=733$ MeV/c, this has already been illustrated in Figs. 2(c)–2(f). For the four lower beam momenta, which are 656 MeV/c, 550 MeV/c, 472 MeV/c, and 404 MeV/c, the

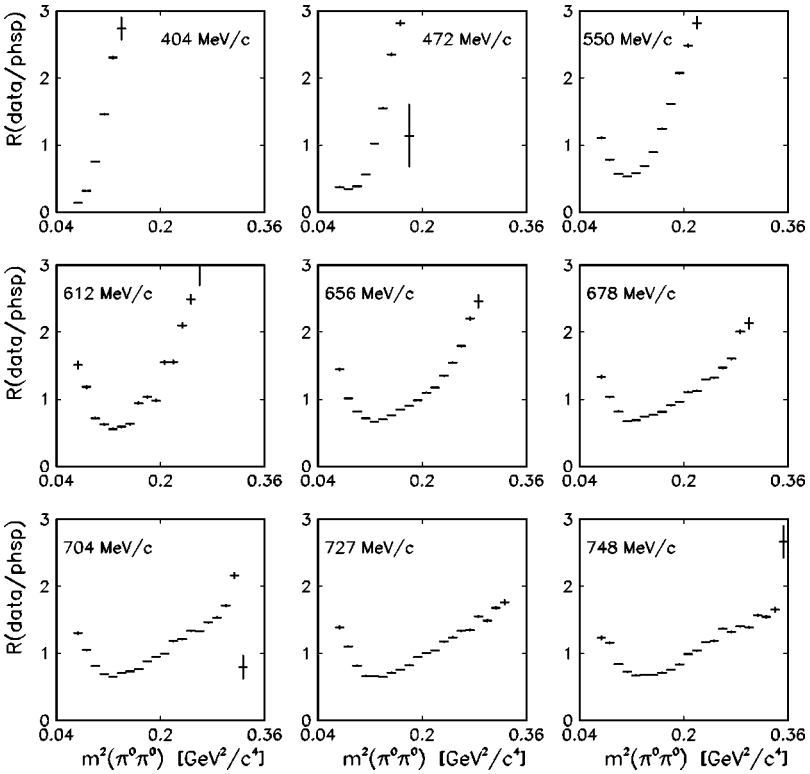

FIG. 7. The ratio of the experimental $m^2(\pi^0\pi^0)$ spectrum and its phase-space distribution for the nine beam momenta shown in Fig. 5.

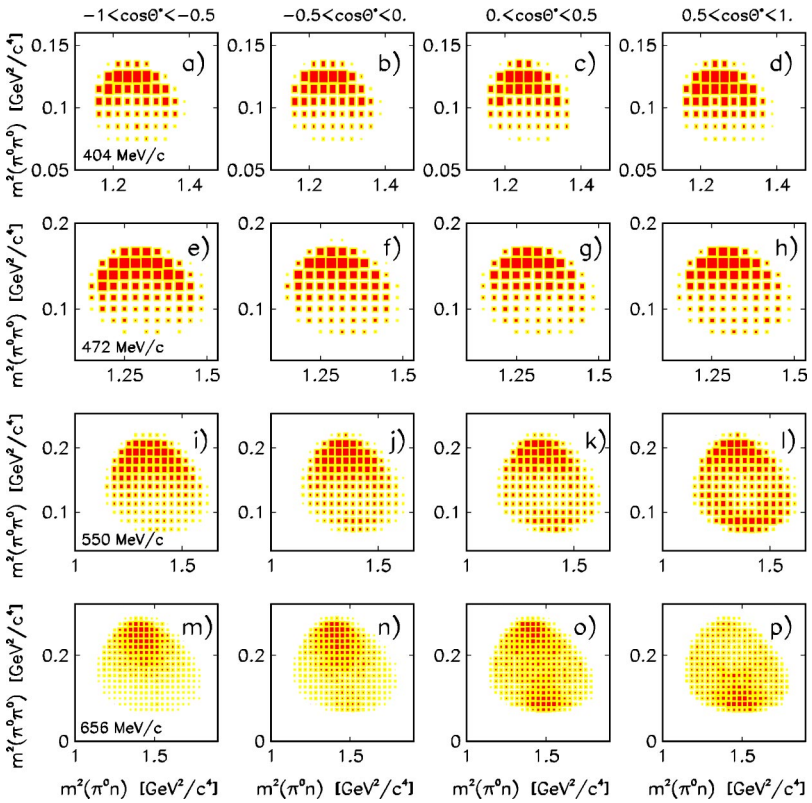

FIG. 8. (Color online) The variation in the experimental Dalitz plots for four different intervals of $\cos\theta^*$ at four different beam momenta. $p_{\pi^-}=404$ MeV/c: (a) $-1<\cos\theta^*<-0.5$, (b) $-0.5<\cos\theta^*<0$,(c) $0<\cos\theta^*<0.5$, and (d) $0.5<\cos\theta^*<1$, $p_{\pi^-}=472$ MeV/c: (e), (f), (g), and (h), $p_{\pi^-}=550$ MeV/c: (i), (j), (k), and (1), $p_{\pi^-}=656$ MeV/c: (m), (n), (o), and (p). The order of the $\cos\theta^*$ intervals for each momentum is the same.

corresponding Dalitz plots are shown in Fig. 8.

For all data above $p_{\pi^-}=550$ MeV/c, a strong dependence of the $m(\pi^0\pi^0)$ spectrum on the $2\pi^0$ production angle is seen. For backward $2\pi^0$ angles, there is an enhancement of the experimental events for large $m(\pi^0\pi^0)$ masses. For forward $2\pi^0$ angles, the situation is opposite; there is an enhancement for small $m(\pi^0\pi^0)$ masses. For the data below $p_{\pi^-}=550$ MeV/c, the dependence of the Dalitz plot density on the $2\pi^0$ production angle is small; there is an enhancement of the experimental events at large $m(\pi^0\pi^0)$ masses for all four $\cos\theta^*$ intervals.

To illustrate the change of the $\cos\theta^*$ distributions with the beam momentum, we show in Fig. 9 these distributions for nine different momenta of the LH_2 data. These distributions are shown in units of mb/sr, so they can be considered as the differential cross sections of reaction (1). Details on the determination of the number of beam pions incident on target and the effective number of hydrogen atoms in the target are given in the following section.

The detailed investigation of the $\pi^0\pi^0 n$ dynamics by a partial-wave analysis of the data at all beam momenta simultaneously is foreseen.

VI. NUMBER OF BEAM PIONS AND TARGET PROTONS

Besides the determination of the number of initially produced $\pi^0\pi^0 n$ events, the cross-section calculation also needs the total number of beam pions, N_{π^-}, incident on the target and the effective number of hydrogen atoms in the target. The LH_2 target had a cylindrical shape along the beam direction with hemispherical endcaps. The maximum target thickness of 10.57 cm was along the beam axis. The hemisphere radius was 7.62 cm. The effective hydrogen density for the LH_2 conditions calculated in units of (mb cm)$^{-1}$ is $\rho^{\mathrm{Eff}}_{\mathrm{LH_2}}=4.248\times10^{-5}$. Then, the effective number of hydrogen atoms is $N^{\mathrm{Eff}}_{\mathrm{LH_2}}=\rho^{\mathrm{Eff}}_{\mathrm{LH_2}}\times l^{\mathrm{Eff}}_{\mathrm{LH_2}}$, where $l^{\mathrm{Eff}}_{\mathrm{LH_2}}$ is the effective thickness of the LH_2 target for the π^- beam passing through the entire target. This effective thickness was determined by a MC simulation, where the real beam-trigger events were used for calculating the average path length through the target. Taking into account the spatial distribution of the data at different beam momenta, the effective number of hydrogen atoms in the LH_2 target is $N^{\mathrm{Eff}}_{\mathrm{LH_2}}=(4.05\pm0.08)\times10^{-4}$ mb^{-1}. The calculation of the effective number of hydrogen atoms in the CH_2 targets was easier due to the cylindrical shape of these targets. For the CH_2 target with thickness 1 cm, this number was 0.806×10^{-4} mb^{-1}; for the 2-cm-thick target, it was 1.621×10^{-4} mb^{-1}; and the 3-cm-thick target was just a sum of the first two.

The calculation of N_{π^-} involves several corrections that take into account scattering and decay of pions, and also the contamination of the pion beams by muons and electrons. The decay and scattering of the beam pions can be taken into account by simulation. The real beam-trigger events were used as input for this simulation. The trajectory parameters for the beam particles were measured by the drift chambers located in the beam line. For beam momenta below 350 MeV/c, the beam contamination by muons and electrons can be measured by a time-of-flight (TOF) system. The muon contamination was 2%–4% for beam momenta above 400 MeV/c [13]. For all momenta, the electron contamination was also investigated using a Čerenkov counter located in the beam downstream of the CB. However, the analysis of

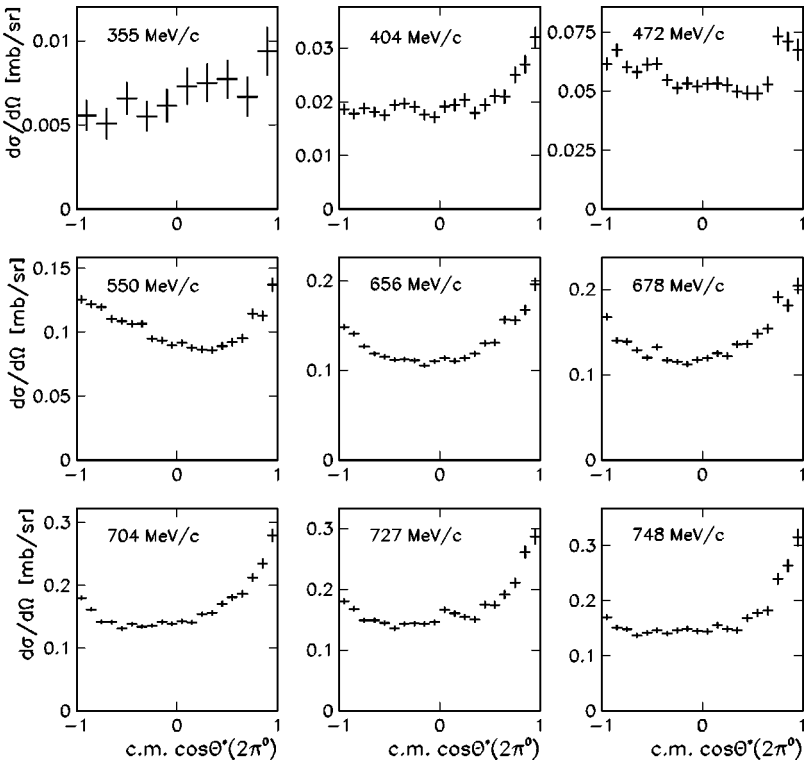

FIG. 9. Differential cross sections for the $2\pi^0$ system produced in reaction $\pi^- p \to \pi^0 \pi^0 n$. They are given for the LH_2 data at nine different beam momenta.

the LH_2 data at $p_{\pi^-} < 350$ MeV/c revealed an inconsistency between the beam contamination by electrons as determined by the TOF system and by the Čerenkov counter. The results determined by the Čerenkov counter were systematically lower. In this energy range, there are several measurements of the charge-exchange (CEX) reaction $\pi^- p \to \pi^0 n$. Comparison of our results for the CEX reaction with the existing data showed good agreement for the only case when the beam contamination was determined using the TOF information [14]. For higher momenta, where only Čerenkov counter information was available, our results for the CEX reaction also turned out to be below the existing data. An additional study was carried out to understand this problem. It turned out that using a separator to eliminate the electrons from the pion beam resulted in a small deviation between the directions of the pion and electron parts of the beam. This deviation did not matter when the beam was triggered by the system of scintillation counters located upstream of the CB. However, the large distance to the Čerenkov counter, which was located 8 m downstream of the target, resulted in a considerable shift between the pion and electron parts. Since the separator was usually tuned to have the lowest rate in the Čerenkov counter, it merely led to the case where the maximum of the electron part of the beam was not in the fiducial volume of the Čerenkov counter.

The second part of the experiments, which was performed with the solid targets, was optimized to minimize the uncertainties in the beam control. Instead of the separator, a 3-mm-thick lead plate was used to suppress the beam contamination by electrons. Using the solid targets allowed us to put an extra beam counter located just 30 cm upstream of the target. The transverse size of the counter, 5×5 cm^2, and its thickness of 5 mm insured that the pions which triggered the beam also hit the target. The losses due to nuclear interactions of the beam pions in the counter and their decay along the 30-cm distance were very small. The Čerenkov counter was moved upstream to be as close as possible to the CB; its new location was just 2.5 m downstream of the target. Also for beam momenta above 690 MeV/c, the measurements were repeated with the target shifted upstream from the CB center. This shift improved the CB acceptance for π^0's produced in the forward direction. The second part of the experiments covered only the energy range $p_{\pi^-} \geqslant 470$ MeV/c, but with more points in the region of the Roper resonance. The beam contamination by electrons, according to the Čerenkov counter information, varied from 12% at the lowest momentum to 3% at the highest momenta. The beam contamination by muons was taken as 3% for all data with $p_{\pi^-} \geqslant 470$ MeV/c (see Ref. [13]).

For the LH_2 data with $p_{\pi^-} \geqslant 322$ MeV/c, N_{π^-} was calculated using the normalization to the differential cross section of the CEX reaction. Besides, for the normalization of all LH_2 data with $p_{\pi^-} \geqslant 470$ MeV/c, we used our own results for the CEX reaction obtained from the CH_2 data. In Fig. 10 we illustrate the normalization for the case where the beam momentum, which is 656 MeV/c, is the same for both the LH_2 and CH_2 data. In the same figure we also show the corresponding FA02 solution of SAID [15], which is an output of the partial-wave analysis (PWA) of the George Washington group based on experiments made earlier by many other groups.

To exclude the effect of the low acceptance in the forward angles for all momenta at and above 470 MeV/c, we excluded from normalization the angular range $\cos \theta^*_{\pi^0} > 0.6$, where $\theta^*_{\pi^0}$ is defined as the angle between the π^0 and the beam direction in the overall c.m. system. Note that the LH_2 data are in better agreement with the PWA solution for the forward and backward angles, where the CH_2 points go

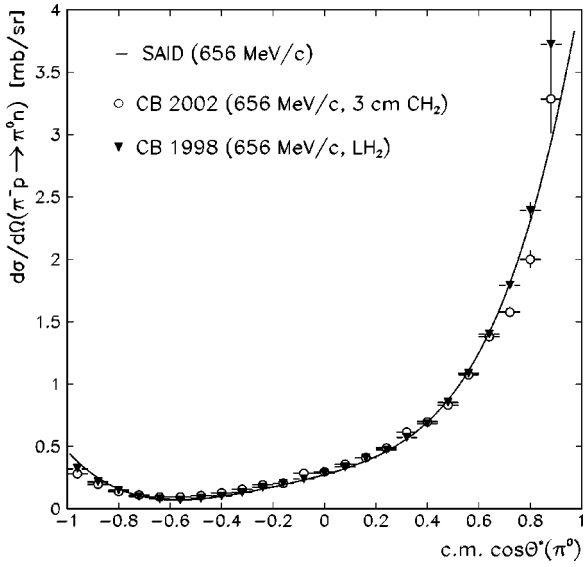

FIG. 10. Differential cross sections for reaction $\pi^- p \to \pi^0 n$ at $p_{\pi^-} = 656$ MeV/c. The LH_2 data are normalized to the middle angles ($-0.8 < \cos\theta^*_{\pi^0} < 0.6$) of the CH_2 data, where the agreement is better. The PWA solution is taken from the SAID data base.

slightly below the LH_2 ones. We explain this by the fact that the CH_2 data were taken at much larger beam intensity than the LH_2 data. As discussed above, in that condition we cannot avoid some losses of good events caused by the overlap of the true and pileup clusters. Since the pileup clusters mostly occur in the crystal layers surrounding the beam line, the forward and backward π^0 production is most sensitive to these losses. An example of the normalization when the beam momentum was slightly different for the CH_2 and LH_2 data is illustrated in Fig. 11, where the beam momenta for the CH_2 and LH_2 data were 738 MeV/c and 733 MeV/c, respectively.

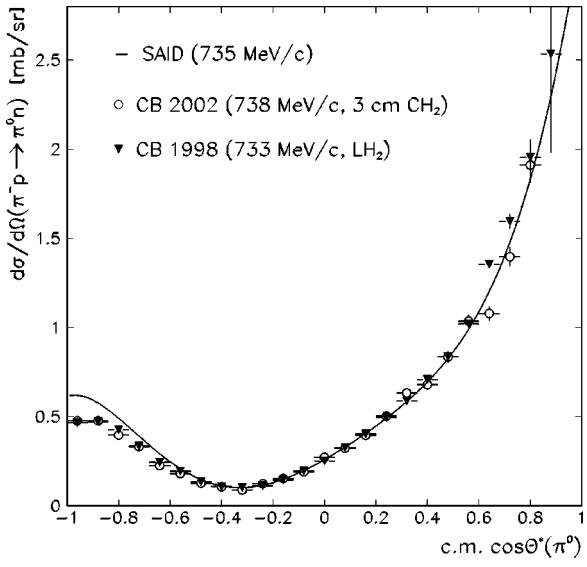

FIG. 11. Differential cross sections for reaction $\pi^- p \to \pi^0 n$ for beam momenta close to $p_{\pi^-} = 735$ MeV/c. The method of the LH_2 data normalization is given in the text. The PWA solution for $p_{\pi^-} = 735$ MeV/c is taken from the SAID data base.

The PWA solution is shown in the same figure for the intermediate $p_{\pi^-} = 735$ MeV/c. Note that our results disagree with the PWA solution for the backward angles, although much better agreement is seen for the middle angles. Therefore, our normalization required that the ratio of the PWA solution at $p_{\pi^-} = 738$ MeV/c to the CH_2 data was the same as the ratio of the PWA solution at $p_{\pi^-} = 733$ MeV/c to the LH_2 data. Only the middle part of the cos $\theta^*_{\pi^0}$ distributions was used to get these ratios. Note that for the entire energy range of the CH_2 data, our agreement with the PWA solution for the CEX reaction is very reasonable; the difference is only seen in the backward angles for momenta above $p_{\pi^-} = 700$ MeV/c. Our results for the LH_2 data at low momenta, where the beam contamination was determined from the TOF information, also show good agreement with the PWA solution for the CEX reaction; therefore, we decided to normalize our three remaining momenta on LH_2 data (i.e., $p_{\pi^-} = 355$ MeV/c, 373 MeV/c, and 404 MeV/c) to the corresponding solution of the PWA for the CEX reaction.

VII. CROSS SECTIONS AND THEIR SYSTEMATIC UNCERTAINTIES

The main results for the total cross section $\sigma_t(\pi^- p \to \pi^0 \pi^0 n)$ are listed in Table I. All results obtained with the LH_2 data are included in Table I, since these data have less background and much larger statistics than the CH_2 data. The CH_2 results we consider to be supplementary to help with the normalization of the LH_2 data and with the evaluation of the systematic uncertainties of the measurement. The CH_2 results are given in Table II except for the beam momenta of 501 MeV/c and 612 MeV/c, which were included in the main table, since there were no corresponding measurements with the LH_2 target. The uncertainties that are given for the total cross section in the tables are the statistical ones only.

Our results for the total cross section $\sigma_t(\pi^- p \to \pi^0 \pi^0 n)$ are shown in Figs. 12 and 13 as a function of the beam momentum. The existing data are shown in the same figures.

Note that the statistical uncertainties for our high momenta are much smaller than for the existing data. For low momenta we have good agreement with the most recent data. The energy dependence of our total cross section $\sigma_t(\pi^- p \to \pi^0 \pi^0 n)$ is in good accord with the expectation that the largest contributions to this channel are the $N(1440)$ and the $N(1520)$. The maximum which the total cross section reaches at $p_{\pi^-} = 730$ MeV/c does correspond to the $N(1520)$ mass. A shoulder that is seen in the total cross section at lower momenta appears to be a manifestation of the Roper resonance. The position and the width of this shoulder are in better agreement with the pole parameters [1] of the $N(1440)$ than with the conventional Breit-Wigner mass and width. It is also interesting to compare the energy dependence of our $\sigma_t(\pi^- p \to \pi^0 \pi^0 n)$ results and the relevant cross section of process $\gamma p \to \pi^0 \pi^0 p$ [23]. In Fig. 14 we show the total cross sections for both processes as a function of the c.m. energy. The absence of the Roper-resonance shoulder in the $\gamma p \to \pi^0 \pi^0 p$ cross section is no surprise as the Roper resonance has only a small radiative coupling. Note the difference in

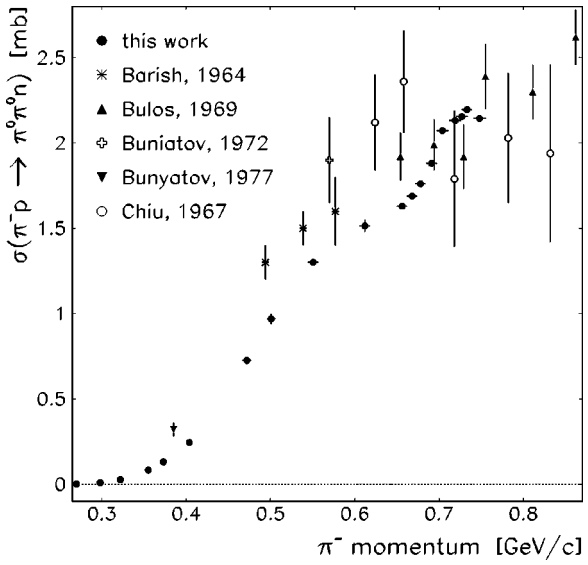

FIG. 12. Total cross section $\sigma_t(\pi^- p \to \pi^0 \pi^0 n)$ as a function of the beam momentum. Our results are compared to prior data [16–20].

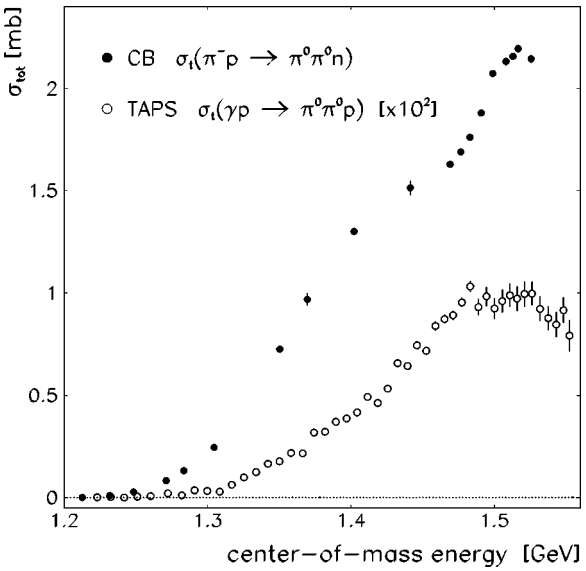

FIG. 14. Total cross section $\sigma_t(\pi^- p \to \pi^0 \pi^0 n)$ compared to $\sigma_t(\gamma p \to \pi^0 \pi^0 p)$ as a function of the c.m. energy.

the dependence of σ_t on the c.m. energy close to the threshold for γ and π^- beams.

Since most of the results for $\sigma_t(\pi^- p \to \pi^0 \pi^0 n)$ obtained with the LH_2 target have a very small statistical uncertainty, the systematic uncertainty becomes the dominant one. As discussed already, the main sources of the systematic uncertainties are the background subtraction, the acceptance correction, and the calculation of the number of incident pions N_{π^-}. Based on the agreement obtained between the SAID CEX results and our measured differential cross section (especially in the middle part of the cos θ^* distribution), the combined systematic uncertainty in our CEX data is 3%–4%. SAID itself can be assigned a 2% uncertainty of its best solution for middle cos θ^*. The middle part of the cos θ^* distribution is almost insensitive to the beam intensity. As discussed above, a high beam intensity causes losses of good events due to the overlap of the pileup and true clusters. Note that several data sets with the CH_2 target were taken with too high beam intensity. This gives slightly lower results for two or three values of $\sigma_t(\pi^- p \to \pi^0 \pi^0 n)$ in Table II; they lie below our main results and the CH_2 results, which have the same beam momentum and a lower beam intensity. For the same data sets of high beam intensity, similar losses are seen in forward and backward angles of the differential cross section for the CEX reaction. However, the middle part of the cos θ^* distribution did not change. This allows us to consider that our normalization of the LH_2 data to the CH_2 data is not worse than 2%. Since the LH_2 data were taken at low beam intensity, the effect of the pileup losses to the LH_2 results for $\sigma_t(\pi^- p \to \pi^0 \pi^0 n)$ is very small ($<1\%$). Finally, the total systematic uncertainty due to the normalization of the LH_2 data to the CEX reaction measured with the CH_2 target is estimated to be about 5%.

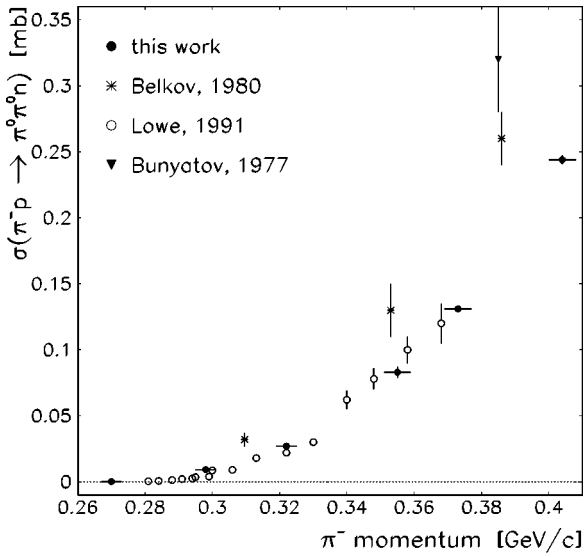

FIG. 13. Total cross section $\sigma_t(\pi^- p \to \pi^0 \pi^0 n)$ as a function of the beam momentum for $p_{\pi^-} < 410$ MeV/c. Our results are compared to prior data [20–22].

Another systematic uncertainty comes from the combined features of the $\pi^0 \pi^0 n$ dynamics and the CB acceptance. Earlier we discussed three methods for calculating the number of initially produced $\pi^0 \pi^0 n$ events. We showed that the average detection efficiency of reaction (1) does not always give the correct result. More reliable results can be obtained by using the cos θ^* distribution or by dividing data into four subsets of cos θ^* with the four Dalitz plots corrected for their acceptance. Since the CB acceptance drops for the forward dipion angles, the latter methods give more accurately the number of initially produced events for the case when the production angular distribution of the $2\pi^0$ system is asymmetric. Note that the difference between the results obtained by the cos θ^* acceptance correction and by the method of four subsets is not larger than 3% over the entire energy range.

For a better understanding of the systematics due to the acceptance correction, some measurements were repeated

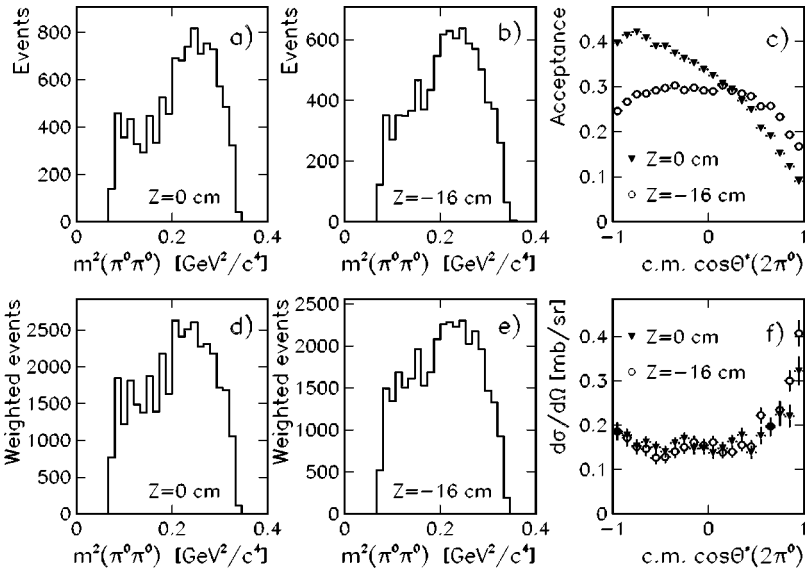

FIG. 15. The experimental distributions for reaction $\pi^- p \to \pi^0\pi^0 n$ at $p_{\pi^-}=738$ MeV/c with the CH_2 target located at the center and 16 cm upstream: (a) the background-subtracted spectrum of $m^2(\pi^0\pi^0)$ when $z_{CH_2}=0$ cm, (b) the background-subtracted spectrum of $m^2(\pi^0\pi^0)$ when $z_{CH_2}=-16$ cm, (c) the acceptance for the $\cos\theta^*$ distribution (shown for both target locations), (d) the $m^2(\pi^0\pi^0)$ spectrum after the acceptance correction when $z_{CH_2}=0$ cm, (e) the $m^2(\pi^0\pi^0)$ spectrum after the acceptance correction when $z_{CH_2}=-16$ cm, (f) the $\cos\theta^*$ distribution after the acceptance correction, calculated in units of differential cross section (shown for both target locations).

with the CH_2 target shifted upstream of the CB center. It gives a larger CB acceptance for forward dipion angles. In Fig. 15 we compare some experimental distributions of reaction (1) that were measured at $p_{\pi^-}=738$ MeV/c with the CH_2 target located at the center of the CB, as well as shifted 16 cm upstream. The beam intensity conditions were almost the same for both measurements.

Because of the limited experimental statistics resulting in large statistical fluctuations after the carbon and the empty-target background subtraction, we show only the $m^2(\pi^0\pi^0)$ projection of the Dalitz plot instead of the plots themselves. In Figs. 15(a) and 15(b) we show the $m^2(\pi^0\pi^0)$ projections that are obtained after background subtraction; they are not yet acceptance corrected. It is seen that the $m^2(\pi^0\pi^0)$ invariant-mass distribution with the target shifted upstream has more events at low masses. This is easy to explain by the earlier observation that low masses $m(\pi^0\pi^0)$ at this momentum are mostly produced in the forward angles. So with the target shifted upstream, such events have a better acceptance. In Fig. 15(c) one can see how different the $\cos\theta^*$ acceptance is for both target locations. In Figs. 15(d) and 15(e) we show the same $m^2(\pi^0\pi^0)$ projections that were obtained as a result of the acceptance correction by using the method of dividing the data into four subsets depending on $\cos\theta^*$. One can see a much better agreement in the mass spectra for both target locations. Finally, in Fig. 15(f) we compare the acceptance-corrected $\cos\theta^*$ spectra obtained for both target locations; these spectra are shown as differential cross sections in units of mb/sr. Within uncertainties, both differential cross sections are in agreement. It is also interesting to compare the total cross sections which are obtained for both target locations with our three methods of the acceptance correction. For the CH_2 target located at the center, the average detection efficiency gives $\sigma_t(\pi^- p \to \pi^0\pi^0 n)=2.07$ mb, the $\cos\theta^*$ acceptance correction gives 2.20 mb, and the method of four subsets gives 2.25 mb. The corresponding values obtained with the CH_2 target located 16 cm upstream are 2.17 mb, 2.28 mb, and 2.29 mb. The statistical uncertainty of all these results is about 0.05 mb. Comparison of these numbers confirms our earlier conclusion that using the average detection efficiency for the cross-section calculation can lead to an underestimate. Applying the $\cos\theta^*$ distribution or the method of four subsets for the acceptance correction has a systematic uncertainty due to this correction of 2%–4%. Finally, the total systematic uncertainty of our total cross sections $\sigma_t(\pi^- p \to \pi^0\pi^0 n)$, which includes all uncertainties mentioned above, is about 6%.

Other systematic uncertainties that we checked were found to be smaller than 1%; so they are not included in the total uncertainty of the measurement. This includes different optimizations of the cluster algorithm, different cluster thresholds, and different confidence levels of the kinematic fit for event selection. Figure 16, for example, illustrates the agreement between the data and MC for the probability distribution of the kinematic fit for the $\pi^- p \to \pi^0\pi^0 n \to 4\gamma n$ hypothesis. The data distribution is the background-subtracted one.

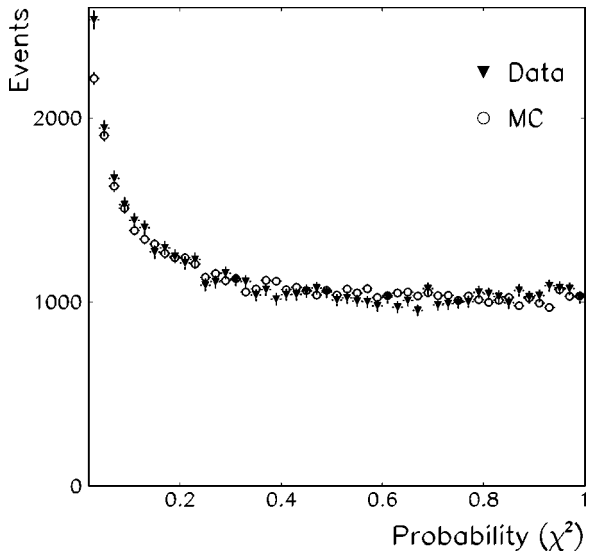

FIG. 16. Comparison of the χ^2 probability distributions for the data and MC events that satisfied the kinematic fit hypothesis for reaction $\pi^- p \to \pi^0\pi^0 n \to 4\gamma n$.

Note that an increase in the distributions for low probability is due to events with partially overlapping photon showers or with a small leakage of energy of the showers into the entrance and exit tunnels of the CB. Since the CB resolution function was determined for "solitary" electromagnetic showers that totally deposited their energy in the CB, it underestimates the errors in the energy and angles of such clusters.

VIII. SUMMARY AND CONCLUSIONS

Reaction $\pi^- p \to \pi^0\pi^0 n$ has been measured with high statistics for 19 incident momenta from threshold to $p_{\pi^-}=750$ MeV/c. The dynamics of the $\pi^- p \to \pi^0\pi^0 n$ reaction and the dependence on the beam energy are shown in total cross sections, Dalitz plots, invariant-mass spectra, and production angular distributions. The Dalitz plots are highly nonuniform; they indicate that the $\pi^0\pi^0 n$ final state is dominantly produced via the $\pi^0\Delta^0(1232)$ intermediate state. There is a strong enhancement at large $m^2(\pi^0\pi^0)$ and a smaller one at low $m^2(\pi^0\pi^0)$ with depletion in between. For beam momenta above 550 MeV/c, the density distribution in the Dalitz plots strongly depends on the angle of the outgoing dipion system (or equivalently on the neutron angle). The production angular distributions are different from the isotropic distribution, and their structure depends on the beam energy. It is remarkable that no direct evidence for a strong $\pi\pi$ interaction in the $I=J=0$ state is seen in $\pi^- p \to \pi^0\pi^0 n$ from threshold to $p_{\pi^-}=750$ MeV/c. A better understanding of the role and contribution of the $f_0(600)$ meson in $\pi^0\pi^0$ production needs a detailed partial-wave analysis of the data. The energy dependence of $\sigma_t(\pi^- p \to \pi^0\pi^0 n)$ shows a shoulder at the Roper resonance, and there is also a maximum near the $N(1520)\frac{3}{2}^-$. It illustrates the importance of these two resonances to the $\pi^0\pi^0$ production process. The $\pi^0\pi^0 n$ cross section is rather large for a reaction with a three-body final state in comparison to a relevant two-body process. Our $\pi^0\pi^0 n$ data implies that the ratio of the total cross sections at $p_{\pi^-}=750$ MeV/c is $\sigma_t(\pi^- p \to \pi^0\pi^0 n)/\sigma_t(\pi^- p \to \pi^0 n) \approx 0.25$. The systematic uncertainty in our total cross sections is about 6%.

ACKNOWLEDGMENTS

This work was supported in part by DOE and NSF, NSERC of Canada, the Russian Ministry of Industry, Science and Technologies, the Russian Foundation for Basic Research. We acknowledge SLAC for the loan of the Crystal Ball. The assistance of BNL and AGS with the setup is much appreciated.

[1] Particle Data Group, K. Hagiwara *et al.*, Phys. Rev. D **66**, 010001 (2002).
[2] M. Olsson and G. B. Yodh, Phys. Rev. **145**, 1309 (1966).
[3] D. Morgan, Phys. Rev. **166**, 1731 (1968).
[4] D. J. Herndon *et al.*, Phys. Rev. D **11**, 3183 (1975).
[5] D. M. Manley *et al.*, Phys. Rev. D **30**, 904 (1984).
[6] V. Bernard, U. Meissner, and I. Zahed, Phys. Rev. Lett. **59**, 966 (1987).
[7] W. Weise, Nucl. Phys. **A553**, 59c (1993).
[8] J. Lowe and H. Burkhardt, πN Newsletter **4**, 102 (1991); **6**, 121 (1992).
[9] K. Craig *et al.*, Crystal Ball Collaboration, Phys. Rev. Lett. **91**, 102301 (2003).
[10] A. Starostin *et al.*, Crystal Ball Collaboration, Phys. Rev. C **64**, 055205 (2001).
[11] W. B. Tippens *et al.*, Crystal Ball Collaboration, Phys. Rev. Lett. **87**, 192001 (2001).
[12] A. Starostin *et al.*, Crystal Ball Collaboration, Phys. Rev. C **67**, 068201 (2003).
[13] W. B. Tippens *et al.*, Phys. Rev. D **63**, 052001 (2001).
[14] M. E. Sadler *et al.*, Crystal Ball Collaboration, Phys. Rev. C (to be published).
[15] R. A. Arndt *et al.*, nucl-th/0311089, Phys. Rev. C (to be published).
[16] B. C. Barish *et al.*, Phys. Rev. **135**, B416 (1964).
[17] F. Bulos *et al.*, Phys. Rev. **187**, 1827 (1969).
[18] S. Buniatov *et al.*, Nucl. Phys. **B42**, 77 (1972).
[19] C. B. Chiu *et al.*, Phys. Rev. **156**, 1415 (1967).
[20] S. A. Bunyatov *et al.*, Sov. J. Nucl. Phys. **25**, 177 (1977).
[21] A. A. Belkov *et al.*, Sov. J. Nucl. Phys. **31**, 96 (1980).
[22] J. Lowe *et al.*, Phys. Rev. C **44**, 956 (1991).
[23] M. Wolf *et al.*, Eur. Phys. J. A **9**, 5 (2000).